Available online at www.sciencedirect.com
SCIENCE DIRECT®
Carbohydrate Research 339 (2004) 1953–1960
Carbohydrate RESEARCH

The conformational free-energy map for solvated neocarrabiose

Kazuyoshi Ueda,[a,*] Tatsuro Ueda,[a] Taiken Sato,[a] Haruo Nakayama[a] and John W. Brady[b,*]

[a]*Department of Material Science, Faculty of Engineering, Yokohama National University, 79-5 Tokiwadai, Hodogaya-ku, Yokohama 240-8501, Japan*
[b]*Department of Food Science, Stocking Hall, Cornell University, Ithaca, NY 14853, USA*

Received 6 October 2003; accepted 28 May 2004

Abstract—A Ramachandran map of the conformational potential of mean force (pmf) for neocarrabiose in water was obtained using molecular dynamics (MD) simulations with umbrella sampling. The potential energy map calculated in a previous study for this molecule in vacuum exhibited a global minimum located at ($\phi = 81°$, $\psi = -141°$). However, the global minimum on the new pmf map in aqueous solution is located in an area centered around ($\phi = 175°$, $\psi = 180°$), indicating a considerable solvent shift. This new global minimum-energy solution conformation was found to correspond to the experimental value obtained from NMR–NOE measurements, and is also consistent with the experimental crystal structure for neocarrabiose and the fiber diffraction conformation for ι-carrageenan. The global minimum of the solution pmf and its local topology were found to be approximately reproduced by quick vacuum conformational energy mapping using several approximations that mimic solvation effects by de-emphasizing intramolecular hydrogen bonding.

1. Introduction

Carrageenans, sulfated copolymers of galactose and anhydrogalactose are widely used in the food industry as gelling and thickening agents.[1] Because of their commercial importance, understanding the conformational behavior of these seaweed polysaccharides is a subject of practical utility, but in spite of considerable effort, the conformations of these molecules remain controversial.[2] We have previously reported molecular mechanics (MM) simulations of carrabiose[3] and neocarrabiose,[4] the unsulfated disaccharide building blocks of the β-carrageenan polymer, as well as MD simulations of a double-helical dimer of two β-carrageenan strands in water.[5] These previous studies indicated that the presence of water can have a strong influence on the conformational structure of the carrageenans, primarily by hydrogen bonding to the sugar hydroxyl groups and replacing carbohydrate–carbohydrate hydrogen bonds. In the case of the double-helical dimer, this competition for hydrogen bond partners destabilized the double helix since the complex was stabilized by hydrogen bonds between the chains, which were replaced by hydrogen bonds to the solvent. In the cases of the disaccharide repeat units, comparison of the vacuum Ramachandran conformational energy map for carrabiose with its solution dynamics behavior found little qualitative change resulting from hydration, consistent with previous work,[6] but a substantial solvation effect was seen in the case of the neocarrabiose repeat unit.

In neocarrabiose, 3,6-anhydro-α-D-galactopyranosyl-(1→3)-β-D-galactopyranose (see Fig. 1), there exists the topological possibility of forming an intramolecular hydrogen bond between the O2 hydroxyl groups of the two rings, designated O2′ for the nonreducing anhydrogalactopyranose ring and O2 for the reducing galactopyranose ring. As a result, this hydrogen bond stabilizes the conformation at ($\phi = 81°$, $\psi = -141°$), which allows it to form, and results in it being the global

* Corresponding authors. E-mail addresses: jwb7@cornell.edu (J.W.B); k-ueda@ynu.ac.jp (K.U)

0008-6215/$ - see front matter © 2004 Elsevier Ltd. All rights reserved.
doi:10.1016/j.carres.2004.05.022

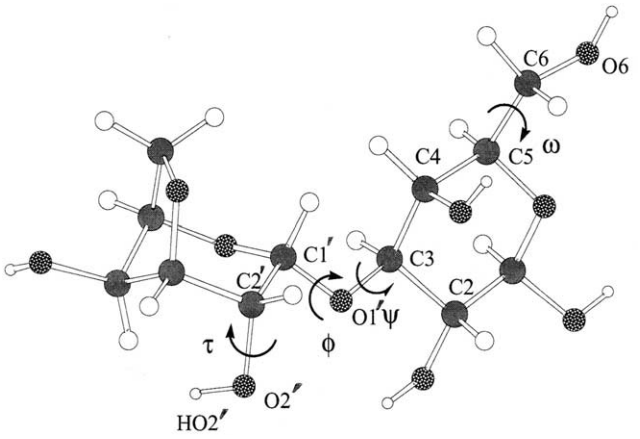

Figure 1. Atomic nomenclature used for neocarrabiose and the notation for the dihedral angles. Note that the designation of the primed and unprimed atoms is opposite to that used in Ref. 4.

minimum-energy geometry on the vacuum Ramachandran energy surface (Fig. 2). However, this conformation is not the one seen in either the experimental crystal structure of neocarrabiose[7] or in the conformation of ι-carrageenan proposed from fiber diffraction.[8–10] While vacuum MD simulations of this disaccharide remained in the various minimum-energy conformations on the vacuum Ramachandran surface, when the molecule was simulated in aqueous solution, the intramolecular hydrogen bonds of the global minimum spontaneously exchanged for hydrogen bonds to solvent as a single water molecule interposed itself between the O2 and O2′ hydroxyl groups, hydrogen bonding to both and bridging between them. The breaking of this internal hydrogen bond produced a shift in the trajectory-averaged stable structure, centering around the two experimental conformations at ($\phi = 175°$, $\psi = 180°$), which is higher in energy on the vacuum map. This result suggests that a Ramachandran free-energy map of the potential of mean force for this disaccharide in aqueous solution would exhibit a significant solvent-induced shift, as was seen in the only solvated disaccharide pmf calculated to date.[11] In order to test this hypothesis, we report here the calculation of such a pmf for hydrated neocarrabiose from an extensive set of MD simulations using umbrella sampling techniques. Because of the enormous computational effort involved, we also compare this map to one calculated using the CHEAT95 force field,[12] a modification of the CHARMM force field, which attenuates hydrogen-bonding interactions as a possible simple approximation of hydration effects.

2. Computational procedures

Conformational maps of the potential of mean force can, in principle, be obtained by averaging the conformational probabilities obtained from MD trajectories of

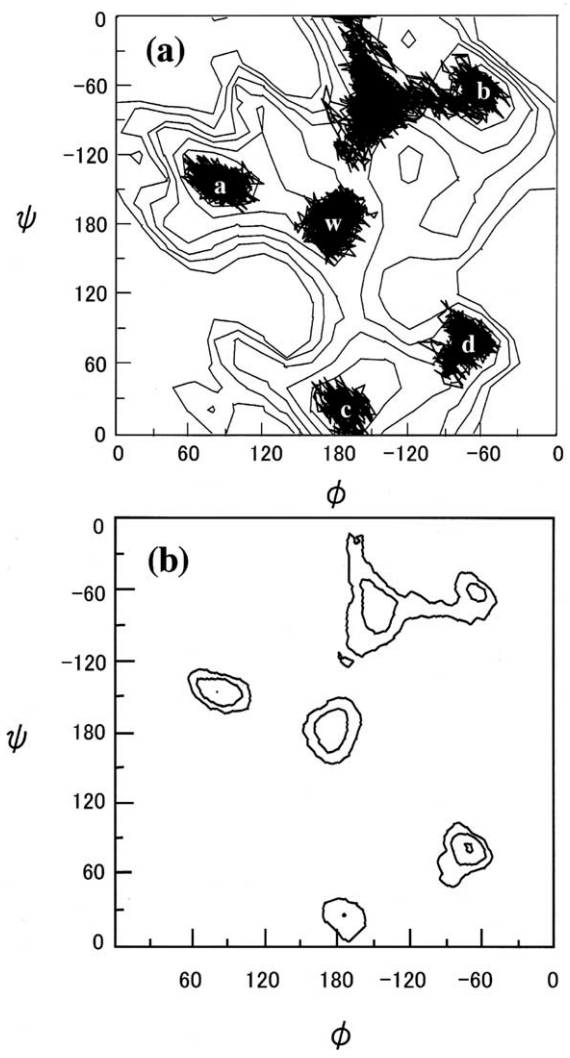

Figure 2. (a) The vacuum adiabatic potential energy map and the trajectories of ϕ and ψ for neocarrabiose in water calculated without any umbrella potential. Five trajectories were started from each of five initial points at the minima of the 'a', 'b', 'c', 'd', and 'w' wells. Each trajectory was 200 ps in length. These trajectories are called the 1st cycle trajectories in the text. (b) The 1st cycle potential of mean force map obtained from the trajectories shown in (a). Contour plots are shown at 1 kcal/mol intervals.

sufficient length. However, in practice this approach is impractical due to the multiple minima on the conformational surface and the tendency for dynamics trajectories (or Monte Carlo simulations) to avoid high-energy conformations, resulting in inadequate statistics for these regions.[13–18] The trajectories started from local energy wells usually remain there because of the short length of the simulations, even though recent advances in computer speeds make possible routine simulations of several nanoseconds. In order to calculate a potential of mean force, information about the relative depths of the free energy wells and the barriers between them is necessary. Umbrella sampling techniques were developed for exactly this purpose,[19] to force systems into high-

energy states for the collection of data for these structures while providing a prescription for later removing the effects of the forcing umbrella potential from the final energy surface. However, the choice of the appropriate umbrella potential is not a simple task, and there is no simple procedure for implementing such calculations.[20,21]

In this study, we first calculated trajectories for the disaccharide in water starting from the energy minima of the previously obtained adiabatic potential energy map.[4] From these trajectories, a first approximation to the map of the potential of mean force in water was calculated. In the next phase, the negative of the first approximation potential energy map was used as an umbrella potential. The iteration of this procedure eventually produced a satisfactorily converged map of the potential of mean force. In each cycle the umbrella potential is stored on a grid as a look-up table, and the umbrella potential at any arbitrary point is determined from a local spline to the potential at the nearest surrounding grid points.

In the simulations reported here, the neocarrabiose disaccharide molecule was placed at the center of a periodic cubic box with a length of 24.65 Å filled with 489 TIP3P[22,23] water molecules. Molecular dynamics simulations were calculated in the NVT ensemble using Langevin dynamics[24] at 300 K with 1 fs time steps using the CHARMM24 program and the HGFB force field for carbohydrates.[25] The conformational probability density function $P^*(\phi,\psi)$ for the simulation using the umbrella function was calculated for $5^\circ \times 5^\circ$ bins over the entire surface of ϕ and ψ by counting the number of configurations in each bin over the duration of each trajectory. The pmf without the biasing umbrella energy function, $W(\phi,\psi)$, can be calculated from the averaged probability density as

$$W(\phi,\psi) = -kT \ln P^*(\phi,\psi) - V_U(\phi,\psi) + C \qquad (1)$$

where V_U is the umbrella potential function. The structure and atomic nomenclature of the neocarrabiose molecule are shown in Figure 1. The glycosidic dihedral torsion angles are defined as ϕ: C2′–C1′–O1′–C3 and ψ: C1′–O1′–C3–C2, respectively. The dihedral angles ω and τ are defined as C4–C5–C6–O6 and C1′–C2′–O2′–HO2′, respectively.

3. Results and discussion

In using umbrella sampling to calculate a pmf efficiently, selecting an appropriate umbrella potential function is important, and in practice, it is necessary to progressively adapt the choice of the functions. In this work, as the first step in this procedure, a rough approximation to the umbrella potential was estimated from unbiased MD trajectories of the molecule in water, without the addition of any umbrella potential. These trajectories were started from minima points found on the vacuum adiabatic potential energy map of this dimer obtained in the previous work.[4] The length of each of these trajectories was 200 ps. The resulting trajectories were then superimposed on the vacuum energy map, as shown in Figure 2a. The three lowest energy minima on the vacuum surface are labeled 'a', 'b' and 'c' in this figure, as in our previous study.[4] The shallow minimum labeled 'd' was not an important minimum on the previously calculated energy map in vacuum, but it was included as a starting point for the first round of simulations because another previous study of neocarrabiose 4^1-sulfate[26] found an apparently stable conformational minimum at point 'd'. The conformation labeled 'w' was identified from our previous simulations in water as the possible minimum free-energy conformation. This point is approximately within the region of the shallow 'e' well on our previous vacuum map,[4] but shifted somewhat by solvation away from that minimum point toward a higher energy region. As can be seen from Figure 2a, the trajectory that started from position 'b' did not stay in this original conformation but moved around a rather wide area of conformation space. The final frame of this trajectory had a glycosidic linkage conformation of ($\phi = -150^\circ$, $\psi = -80^\circ$). However, the other trajectories all remained near their starting points throughout the time simulated. To evaluate the relative depths of these wells, trajectories that adequately sample the barriers between them are required. In these preliminary simulations without umbrella functions, no trajectories sampled these barriers by making transitions between two wells. Therefore, estimations of the relative free energies between the wells could not be evaluated from these trajectories.

Although these five independent simulations cannot provide information about the barriers between the wells, they can be used to approximate the free energy topology within each well. A tentative potential of mean force (pmf) was calculated for these trajectories from Eq. 1 for use as an umbrella potential in the next stage of the calculation. Since the length of each trajectory was the same, these separate pmfs calculated from each trajectory were simply combined as a revision to the vacuum adiabatic map, as shown in Figure 2b. The negative of this tentative pmf was then used as the umbrella potential for a second cycle of molecular dynamics simulations.

MD simulations using this umbrella function were again started from the same five points, and each was integrated for 500 ps. All the trajectories were again superimposed on the adiabatic potential energy map as shown in Figure 3a. Unlike the first simulations, in this cycle a number of barrier crossings were observed. As can be seen in the figure, the combination of these

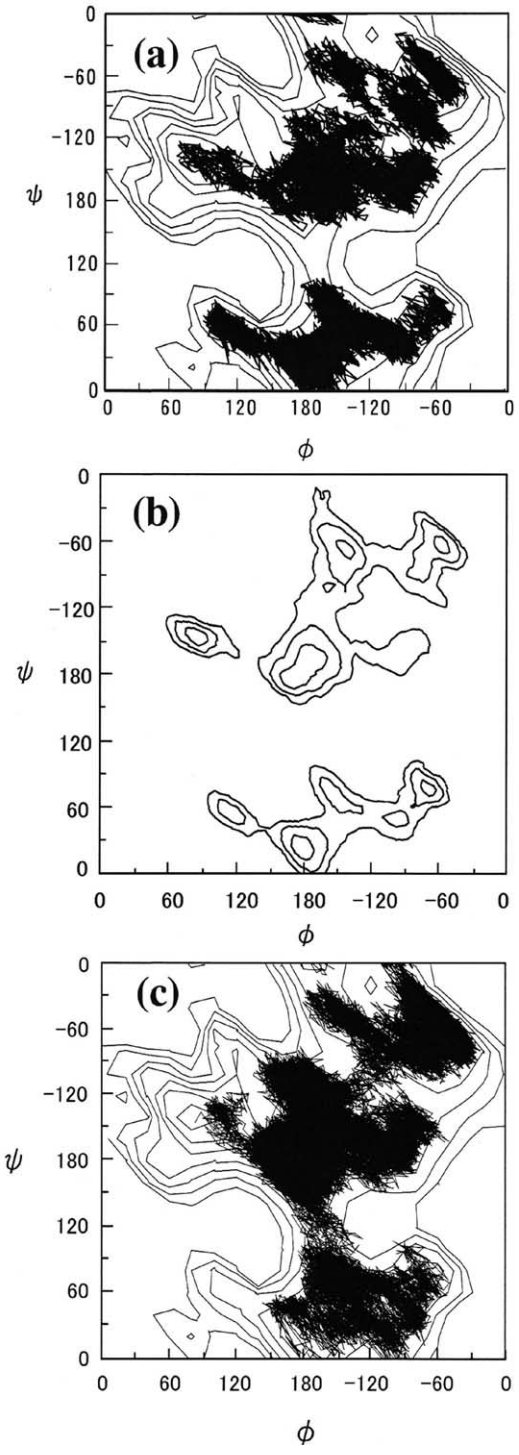

Figure 3. (a) The 2nd cycle trajectories for ϕ and ψ for neocarrabiose in water calculated with an umbrella potential, which was the negative of the 1st cycle potential of mean force. The trajectories shown in the figure are the simple sum of all trajectories started from the five minimum points of the 'a', 'b', 'c', 'd', and 'w' wells. (b) The 2nd cycle potential of mean force map obtained from the trajectories shown in (a). Contours are shown at 1 kcal/mol intervals. (c) The 4th cycle trajectories of ϕ and ψ for neocarrabiose in water calculated using an umbrella potential, which was the negative of the 3rd cycle potential of mean force. The trajectories were started from the 'a', 'c', and 'w' wells, respectively.

trajectories covered most of the area of the sterically allowed (ϕ,ψ) space for this molecule. The (ϕ,ψ) probability densities were calculated from these trajectories and used to construct a second approximation to the pmf map by combining the probability densities using a one-point normalization procedure. The resulting pmf map is shown in Figure 3b. The negative of this pmf map was used again as an umbrella potential in the next iteration step. This procedure was repeated two more times, and the final trajectories for the fifth cycle are shown in Figure 3c.

In this final iteration, three trajectories of 1000 ps each were started from the 'w', 'a', and 'c' points, respectively. All three trajectories are simultaneously superimposed on the adiabatic potential energy map shown in Figure 3c. The combination of these trajectories can be seen to cover virtually all the area of the sterically allowed ϕ,ψ plane. To illustrate the transitions in the trajectories, the histories of ϕ and ψ for the trajectory that started from the 'a' well are shown in Figure 4. As can be seen, both ϕ and ψ undergo transitions and sample a wide range of dihedral angles. The trajectory that started at 'a' moved to the 'w' well after 50 ps of dynamics, where it remained for 300 ps. It then moved to the 'c' well and finally to the 'b' region. Another trajectory that started in the 'c' well is shown in Figure 5a and b. It can be seen that this trajectory stayed in the 'c' well for a short time, but soon moved to the 'b' well and stayed there for about 500 ps. Finally it moved to the 'w' well, where it remained until the end of the simulation. The last trajectory is shown in Figure 5c and d. This simulation started in the 'w' well and remained in the same area throughout the simulation, although it samples a much wider conformational range than the 'w' trajectory shown in Figure 2a. Collectively these trajectories sample the barriers between the wells sufficiently to allow the estimation of their relative energies, as judged from the density of sampling evident in these regions from Figure 3c. The trajectories exhibit a tendency to move toward the 'w' well, and the combined data finds the 'w' energy well to be the global minimum on the free-energy surface.

The rotations of the primary alcohol group and of the various hydroxyl groups are also an important measure of the conformational sampling for adequate statistics. The history of the dihedral torsion angle ω of the primary alcohol group of the reducing-end β-D-galactose ring for the trajectory, which started from the 'a' well is shown in Figure 4c. It can be seen that this primary alcohol group rotated frequently and assumed all three staggered conformations. A typical example of the rotation of the hydroxyl groups is shown in Fig. 4(d), which displays the history of the dihedral angle τ of the hydroxyl group on the C2′ position of the 3,6-anhydro-α-D-galactose from the same simulation. As can be seen, this group rotated frequently, sampling all three stag-

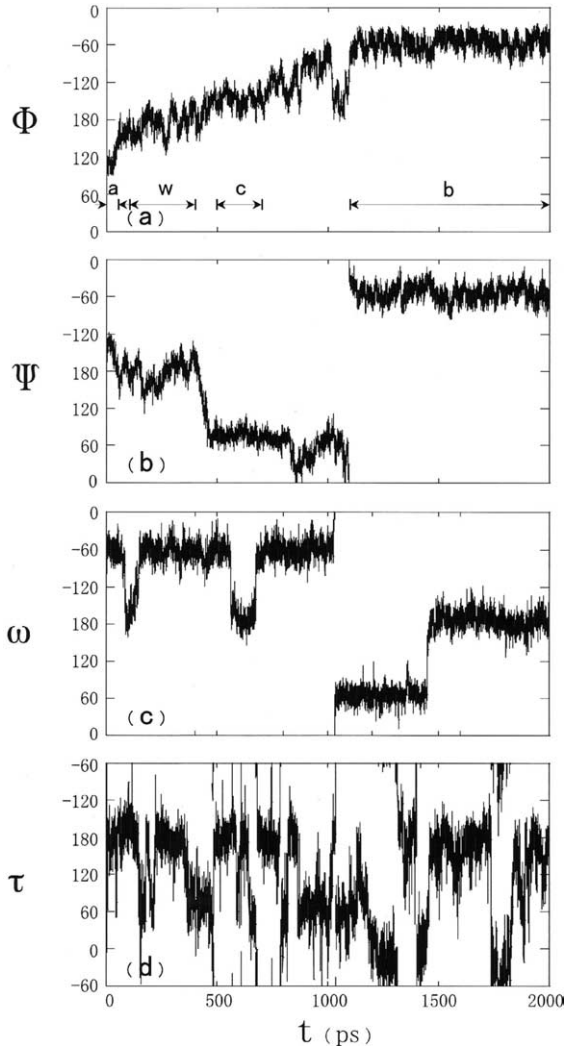

Figure 4. Histories of the (a) ϕ and (b) ψ dihedral angles of the glycosidic linkages of the 4th step trajectories started from the 'a' well. The histories of the dihedral angles of the primary alcohol group ω (c) on the β-D-galactose ring and the hydroxyl group τ on the 2-position of α-D-galactose ring (d) analyzed from the trajectory started from 'a' well are also shown.

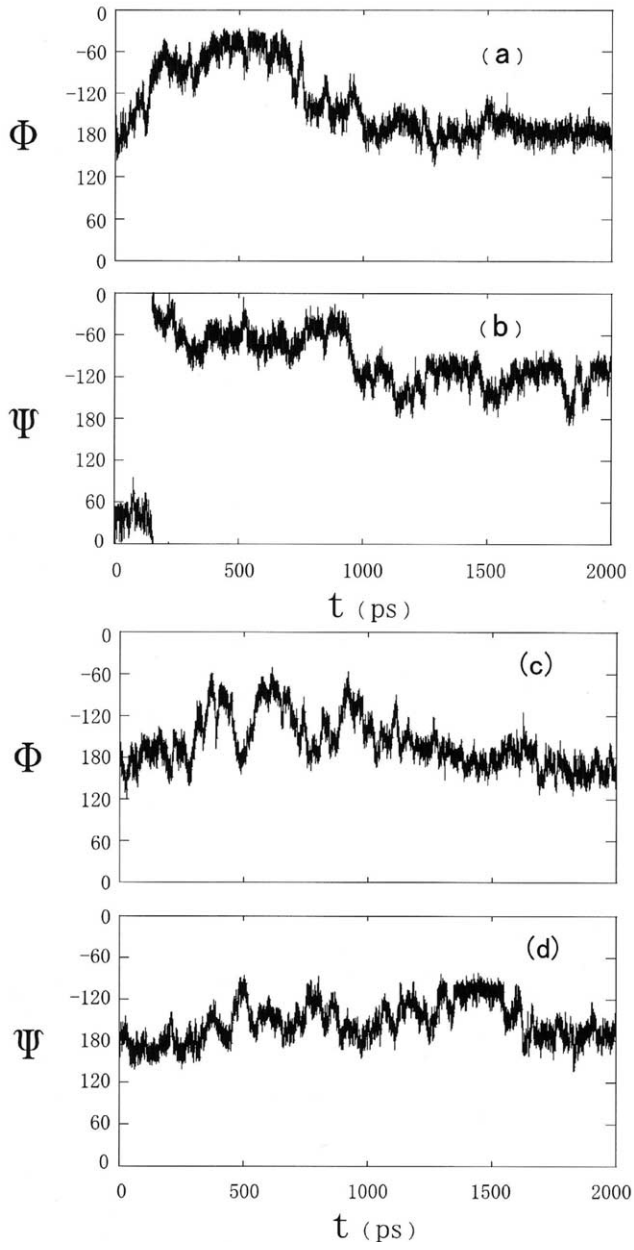

Figure 5. Histories of the (a) ϕ and (b) ψ dihedral angles of the glycosidic linkages of the 4th step trajectories, which started from the 'c' well, and the histories of the (c) ϕ and (d) ψ dihedral angles of the glycosidic linkages of the 4th step trajectories, which started from the 'w' well.

gered positions. These rotations indicate that the possible conformations of neocarrabiose are well sampled by the simulations in water.

The final potential of mean force map was calculated from the trajectories shown in Figure 3c and is shown in Figure 6a. It can be seen that the global minimum is no longer at 'a' but rather at 'w'. The values of the potential of mean force for five local minima at each iteration step are summarized in Table 1. Although the global minimum is located at 'd' in the first cycle, it shifted to 'a' in the second cycle and then to the 'w' well in all of the subsequent steps as the iteration procedure gradually improved the calculated pmf, and the relative free energy for the 'w' well gradually decreased throughout this process. Conversely, the depth of the 'a' well sharply diminished throughout the iteration procedure, although this well was the global minimum on the vacuum adiabatic potential energy map. This shift in the global minimum from 'a' to 'w' is thus the result of the aqueous environment.

The final pmf map can be compared to vacuum maps that use various approximations to mimic a water environment. One such map can be calculated simply by using a dielectric constant higher than unity, which will, among other things, have the effect of decreasing

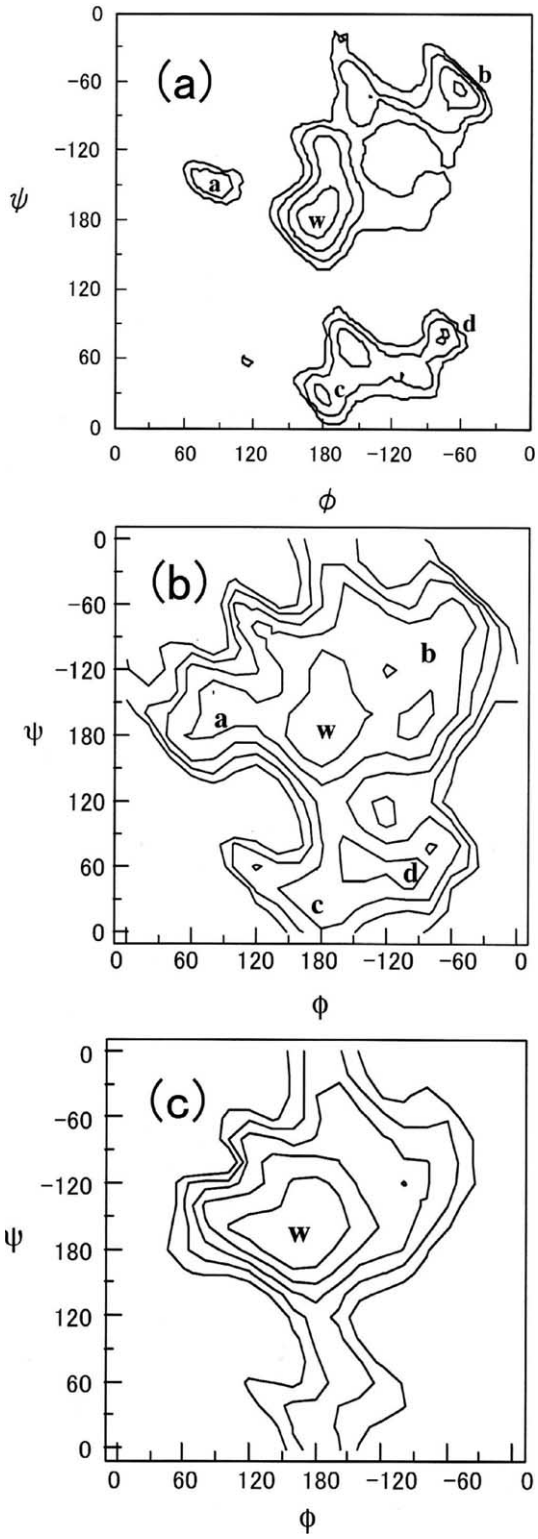

Figure 6. (a) The final, 4th step potential of mean force map obtained from the trajectories shown in Fig. 3(c). Contour are shown at 1 kcal/mol intervals. (b) Adiabatic potential energy map calculated using the Ha et al. potential function with a dielectric constant $\varepsilon = 4$; and (c), using the CHEAT95 potential. Contour are shown at 2 kcal/mol intervals.

intramolecular hydrogen bonding. Figure 6b shows such a map that was calculated using $\varepsilon = 4$. On this map, the global minimum is again located not at 'a' but at 'w', as on the hydrated pmf. Another such map can be calculated by using the CHEAT95 potential,[12] which replaces sugar hydroxyl groups with extended atoms, which also has the effect of eliminating intramolecular hydrogen bonding and mimicking hydration effects. The CHEAT95 map is shown in Figure 6c. Although the overall potential shape is simpler than the previous one, the location of the global minimum point is almost the same. The location of these minima and their relative potential energies are also listed in Table 1. It is also worth noting that the global minimum found here is similar to that found in previous conformational energy studies using alternate force fields and approximations.[7,27,28] These results indicate that the global minimum-energy conformation of this dimer is strongly affected by the reduction of intramolecular hydrogen bonding through competition from solvent water, as suggested in our previous study. Fortunately, the global minimum for this dimer may be estimated from very inexpensive vacuum calculations by using simple approximations to mimic the effects of solvation, although determining the detailed shape of the potential surface requires a detailed treatment of aqueous solvation.

The reduction of intramolecular hydrogen bonding is evidently caused by competition for hydrogen bonds to water molecules. The number of hydrogen bonds in different wells formed between water and the sugar was calculated using the trajectory that started from the 'a' well, for the interval in each well, as shown in Figure 4. The results are given in Table 2. It can be seen that the total number of hydrogen bonds between water and solute is highest in the 'w' well conformation. This indicates that the conformation in the 'w' well is stabilized more by hydration than the other conformations. Among these hydrogen bonds, some form a water bridge between two hydroxyl oxygens of the adjacent sugar rings. The formation of such water bridges was analyzed for various conformations observed in this same trajectory, and the results are listed in Table 3. The formation of such a water bridge occurred most frequently when the molecule was in the 'w' conformation. The most typical water hydrogen bond bridge was formed between O2 and O2′, as was found in our previous work.[4]

4. Conclusions

The calculation of the potential of mean force reported here required considerable simulation time to converge, as in the case of the xylose disaccharide previously studied,[11] but with the recent advances in computer speeds the computational time is not prohibitive. In this case, a strong influence of solvation on the conforma-

Table 1. Comparison of the relative energy values of the five principal local minima for the intermediate and final potentials of mean force obtained for neocarrabiose in water during each iteration stage of the umbrella sampling procedure

Local minimum	ϕ (deg)	ψ (deg)	Vacuum $\varepsilon = 1$ (kcal/mol)	Vacuum $\varepsilon = 4$ (kcal/mol)	CHEAT95 (kcal/mol)	Potential of mean force (kcal/mol)			
						1st	2nd	3rd	4th
a	80	−145	0.0	1.8	—	0.10	0.00	0.16	1.72
b	−60	−65	3.2	2.9	—	0.79	0.36	0.76	0.54
c	180	30	3.7	3.2	—	1.07	0.13	0.26	1.35
d	−75	75	—	2.8	—	0.00	0.17	0.77	1.59
w	170	180	5.4	0.0	0.0	0.38	0.08	0.00	0.00

The minimum energy values obtained for the vacuum map using dielectric constants $\varepsilon = 1$ and 4, and using the CHEAT95 potential, are also shown for comparison (see text).

Table 2. Average number of hydrogen bonds to solvent made by each sugar oxygen atom, as calculated from the trajectory that started from the "a" well, for the time period spent in each well

Atom	Number of hydrogen bonds			
	a conformation (0–50 ps)	w conformation (100–400 ps)	c conformation (500–700 ps)	b conformation (1100–2000 ps)
O1′	0.52	1.26	1.34	1.08
O2′	1.98	2.97	2.77	2.49
O4′	2.61	2.66	2.52	2.82
O5′	0.25	0.83	0.88	1.32
O6′	1.12	0.85	1.03	1.02
O1	2.93	2.99	2.87	2.70
O2	2.28	2.72	2.67	2.05
O4	2.60	2.65	1.83	2.37
O5	0.88	0.81	0.85	1.02
O6	2.11	2.75	2.87	2.97
Total	17.28	20.49	19.63	19.84

Table 3. Comparison of the frequency of occurrence of hydrogen bonded water molecules bridging between hydroxyl groups on different sugar rings of the disaccharide, as calculated from the trajectory that started from the 'a' well

Hydroxyl pair bridged by a hydrogen bonded water molecule	Percentage of the total trajectory time spent in each well			
	a (0–50 ps)	w (100–400 ps)	c (500–700 ps)	b (1100–2000 ps)
O2′–O2	27.2	83.2	55.0	3.1
O2′–O4	0.0	9.5	0.0	0.2
O5′–O2	0.0	19.7	0.0	0.0
O5′–O4	0.0	0.0	1.8	33.6
O5′–O6	0.4	0.7	0.6	0.0

tional energy made the effort worthwhile. As was expected from previous modeling studies of neocarrabiose,[4,6] the pmf in aqueous solution was found to exhibit a significant solvation-induced shift in the global minimum free-energy conformation from that expected in vacuum. This observed conformational shift is consistent with the limited available experimental data. Lamba et al.[7] measured NMR–NOEs for neocarrabiose in water and observed a large signal between the H1′ and H3 atoms. Our previous work[26] found large inter-residue NOE signals between H1′ and βH4 and between H1′ and βH3 of the related neocarrabiose 4^1-sulfate in water. Bosco et al.[29] also observed strong NOE signals between these same aliphatic protons in κ-carrageenan. All of these NOE constraints are satisfied by the global minimum free-energy conformation, 'w', on the Ramachandran energy map calculated here. In addition, this conformation is close to both the crystal structure for neocarrabiose[7] and to the fiber diffraction conformation for ι-carrageenan.[8–10]

It is not expected that a solvation shift such as observed here for neocarrabiose will be observed in all disaccharides. Simulations of carrabiose, for example, suggest that there would not be a significant solvation shift for this disaccharide,[3,6] and in general it may not be possible to determine from inspection in advance, which disaccharides will require a full treatment of solvation in order to produce a realistic solvated conformational

energy map. For this reason, it is encouraging that the two simple approximations to reduce the strength of intramolecular hydrogen bonds that were studied both gave a quick and reliable approximation of the global minimum-energy conformation.

Acknowledgements

The authors thank K. Naidoo for many helpful discussions and S. Paoletti for sharing NOE data for κ-carrageenan in advance of publication.

References

1. Dziezak, J. D. *Food Technol.* **1991**, 116–132.
2. Ueda, K.; Itoh, M.; Matsuzaki, Y.; Ochiai, H.; Imamura, A. *Macromolecules* **1998**, *31*, 675–680.
3. Ueda, K.; Brady, J. W. *Biopolymers* **1997**, *41*, 323–330.
4. Ueda, K.; Brady, J. W. *Biopolymers* **1996**, *38*, 461–469.
5. Ueda, K.; Imamura, A.; Brady, J. W. *J. Phys. Chem. A* **1998**, *102*, 2749–2758.
6. Urbani, R.; Blas, A. D.; Cesàro, A. *Int. J. Biol. Macromol.* **1993**, *15*, 24–29.
7. Lamba, D.; Segre, A. L.; Glover, S.; Mackie, W.; Sheldrick, B.; Peréz, S. *Carbohydr. Res.* **1990**, *208*, 215–230.
8. Arnott, S.; Scott, W. E.; Rees, D. A.; McNab, C. G. A. *J. Mol. Biol.* **1974**, *90*, 253–267.
9. Janaswamy, S.; Chandrasekaran, R. *Carbohydr. Res.* **2001**, *335*, 181–194.
10. Janaswamy, S.; Chandrasekaran, R. *Carbohydr. Res.* **2002**, *337*, 523–535.
11. Naidoo, K. J.; Brady, J. W. *J. Am. Chem. Soc.* **1999**, *121*, 2244–2252.
12. Kouwijzer, M. L. C. E.; Grootenhuis, P. D. J. *J. Phys. Chem.* **1995**, *99*, 13426–13436.
13. Torrie, G. M.; Valleau, J. P. *J. Comput. Phys.* **1977**, *23*, 187–199.
14. Valleau, J. P.; Whittington, S. G. In *Statistical Mechanics. Part A: Equilibrium Techniques*; Berne, B. J., Ed.; Plenum: New York, 1977; pp 137–168.
15. Beveridge, D. L.; DiCapua, F. M. *Annu. Rev. Biophys. Biophys. Chem.* **1989**, *18*, 431–492.
16. Beveridge, D. L.; DiCapua, F. M. In *Computer Simulation of Biomolecular Systems: Theoretical and Experimental Applications*; van Gunsteren, W. F., Weiner, P. K., Eds.; ESCOM: Leiden, 1989; pp 1–26.
17. Mezei, M. J. *Comput. Phys.* **1987**, *68*, 237–248.
18. Pangali, C.; Rao, M.; Berne, B. J. *J. Chem. Phys.* **1979**, *71*, 2982–2990.
19. Patey, G. N.; Valleau, J. P. *J. Chem. Phys.* **1975**, *63*, 2334–2339.
20. Straatsma, T. P.; McCammon, J. A. *J. Chem. Phys.* **1994**, *101*, 5032–5039.
21. Marrone, T. J.; Gilson, M. K.; McCammon, J. A. *J. Phys. Chem.* **1996**, *100*, 1439–1441.
22. Jorgensen, W. L.; Chandrasekhar, J.; Madura, J. D.; Impey, R. W.; Klein, M. L. *J. Chem. Phys.* **1983**, *79*, 926–935.
23. Durell, S. R.; Brooks, B. R.; Ben-Naim, A. *J. Phys. Chem.* **1994**, *98*, 2198–2202.
24. Brooks, C. L.; Karplus, M.; Pettitt, B. M. In *Proteins: A Theoretical Perspective of Dynamics, Structure, and Thermodynamics*; Wiley-Interscience: New York, 1988; Vol. LXXI.
25. Ha, S. N.; Giammona, A.; Field, M.; Brady, J. W. *Carbohydr. Res.* **1988**, *180*, 207–221.
26. Ueda, K.; Saiki, M.; Brady, J. W. *J. Phys. Chem. B* **2001**, *105*, 8629–8638.
27. Le Questel, J.-Y.; Cros, S.; Mackie, W.; Peréz, S. *Int. J. Biol. Macromol.* **1995**, *17*, 161–175.
28. Stortz, C. A.; Cerezo, A. S. *J. Carbohydr. Chem.* **2000**, *19*, 1115–1130.
29. Bosco, M.; Segre, A.; Miertus, S.; Paoletti, S. Personal communication, 2001.